# A Single Molecule View of Conformational Switching of DNA Tethered to a Gold Electrode Supporting Information

Eric A. Josephs[†] and Tao Ye[‡,*]
[†]School of Engineering and [‡]School of Natural Sciences
University of California, Merced
5200 North Lake Road
Merced, California 95343

# Contents

# 1  Complete Sequences of DNA Molecules Used

105 bp (short) DNA: `5'- /5ThioMC6-D/ TTT TTG ACC AAC TTT GAA AGA GGA CAG ATG`
`AAC GGT GTA CAG ACC AGG CGC ATA GGC TGG CTG ACC TTC ATC AAG AGT AAT CTT GAC`
`AAG AAC CGG ATA TTC ATT -3'`

503 bp (long) DNA: `5'- /5ThioMC6-D/ TTT TTG ACC AAC TTT GAA AGA GGA CAG ATG`
`AAC GGT GTA CAG ACC AGG CGC ATA GGC TGG CTG ACC TTC ATC AAG AGT AAT CTT GAC`
`AAG AAC CGG ATA TTC ATT ACC CAA ATC AAC GTA ACA AAG CTG CTC ATT CAG TGA ATA`
`AGG CTT GCC CTG ACG AGA AAC ACC AGA ACG AGT AGT AAA TTG GGC TTG AGA TGG TTT`
`AAT TTC AAC TTT AAT CAT TGT GAA TTA CCT TAT GCG ATT TTA AGA ACT GGC TCA TTA`
`TAC CAG TCA GGA CGT TGG GAA GAA AAA TCT ACG TTA ATA AAA CGA ACT AAC GGA ACA`
`ACA TTA TTA CAG GTA GAA AGA TTC ATC AGT TGA GAT TTA GGA ATA CCA CAT TCA ACT`
`AAT GCA GAT ACA TAA CGC CAA AAG GAA TTA CGA GGC ATA GTA AGA GCA ACA CTA TCA`
`TAA CCC TCG TTT ACC AGA CGA CGA TAA AAA CCA AAA TAG CGA GAG GCT TTT GCA AAA`
`GAA GTT TTG CCA GAG GG -3'`
where /5ThioMC6-D/ is the thiol tether.

## 2 Evolution and Stability of MCH monolayer at +600 mV

For each image in Figures S1, S4, and S5 below, images are presented as in the main text: acquired by scanning each line vertically and the horizontal axis being an effective 'time' axis. An arrow points in the direction of increasing time (scanning direction) if temporal information is useful for interpreting the image. Below each figure is the potential applied to the surface at the time the concurrent line was scanned; all voltages are stated with respect to Ag/AgCl reference electrode. Each image is 1 $\mu$m by 1 $\mu$m and displayed with identical false-color contrast. Voltage labels beneath all images in this section where the potential was recorded simultaneously with line scan.
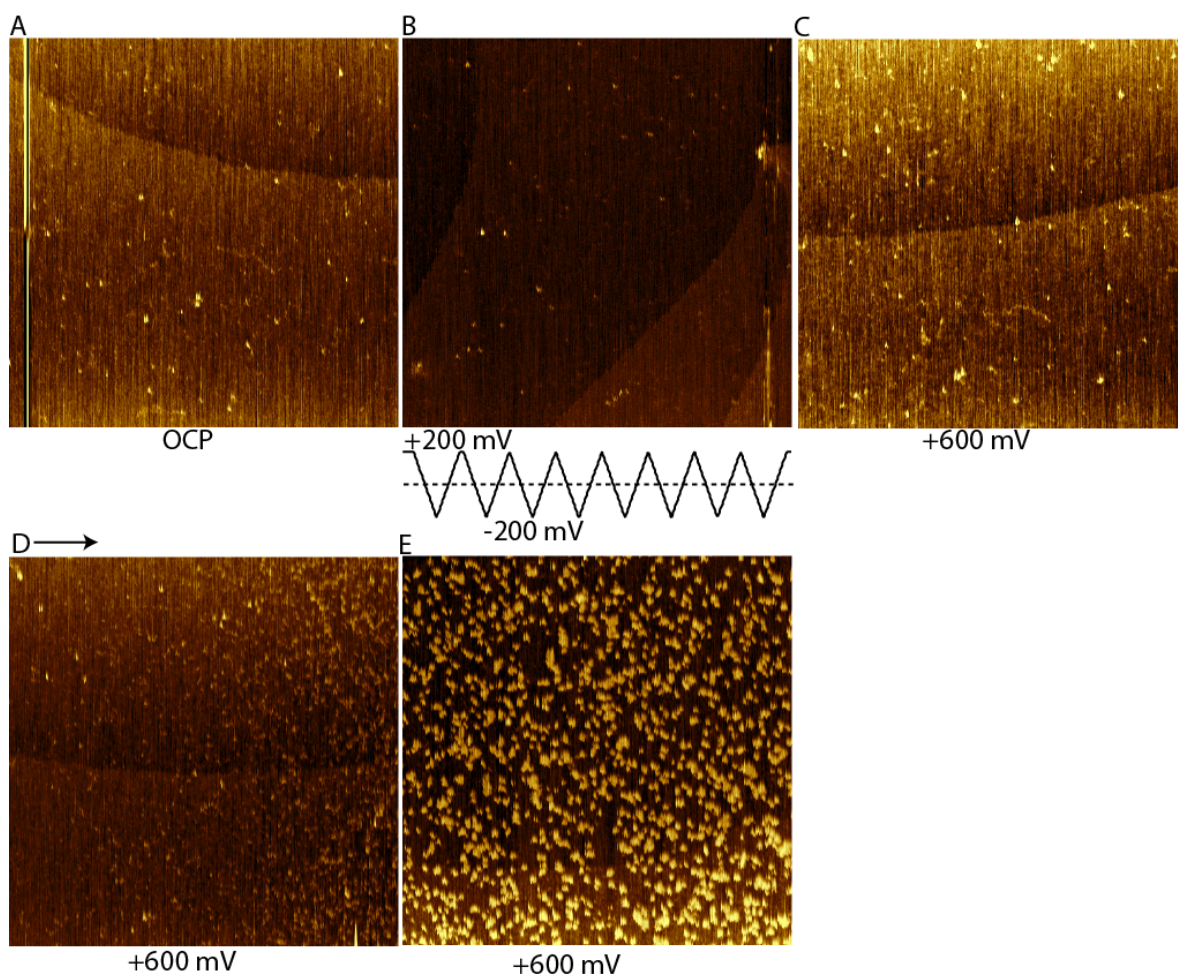
Figure S1: Evolution of MCH monolayer with short DNA upon first application of +600 mV. (A) Prior to beginning the experiment, the surface is imaged at OCP. Few short particles are visible across the surface. (B) During repeated cycling of the potential at 25 mV/sec between +200 mV and -200 mV, the surface appears stationary before application of +600 mV,. (C) When the surface is held at +600 mV during the first scan (5-10 minutes) the morphology of the surface remains approximately the same. (D) Scanning from left to right, we see that with increasing time an increasing number of protrusions appear visible by AFM imaging. Scanning at 1 line/second, the time scale of this transition is on the order of image acquisition. This phenomenon does not occur even if the surface is held at +500 mV (not shown). (E) After a few more more frames of imaging at +600 mV then cycling the potential once from +600 to 0 mV and back, the surface appears saturated with the number of visible protrusions, and DNA appear in the final form apparent in other images.
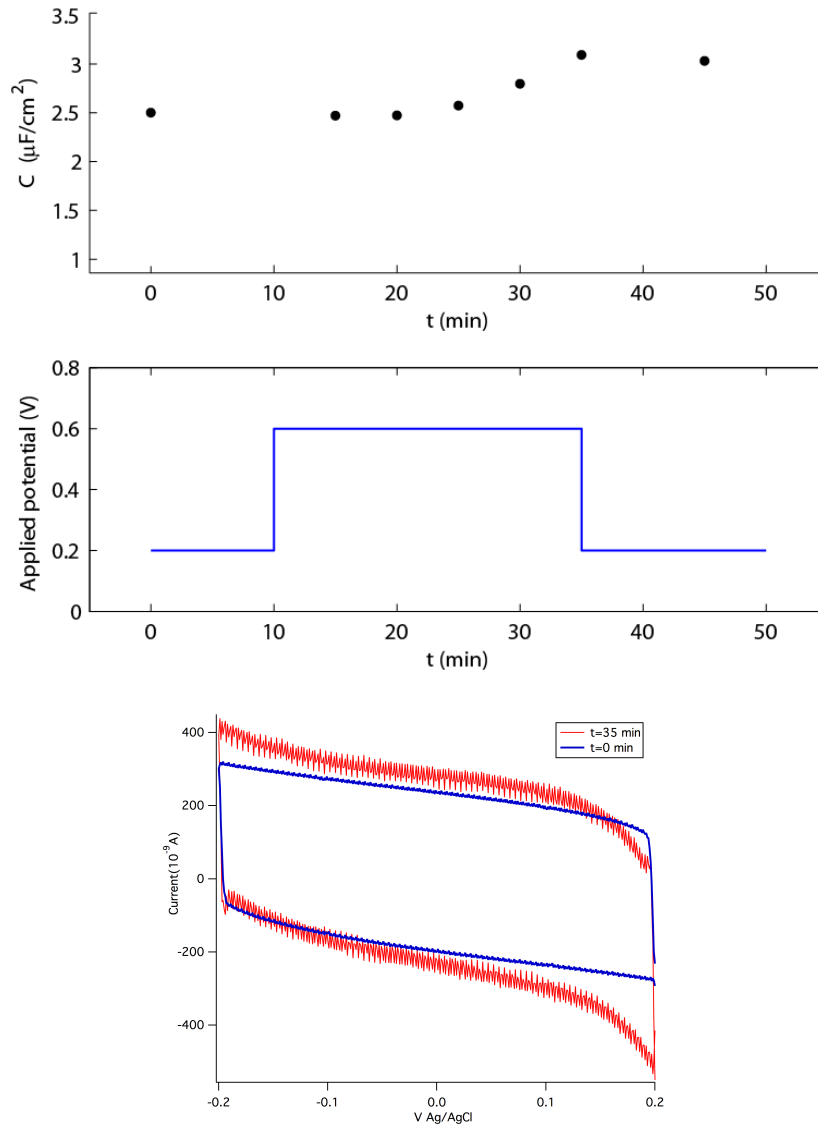
Figure S2: Capacitance of MCH monolayer during treatment at +600 mV (top) during prolonged treatment of +600 mV (middle). Measurements were performed on a single crystal Au(111) surface under 0.5xTAE with MCH monolayer prepared as in the main text. Capacitance was derived from the charging current at 0 mV during a cyclic voltammogram (CV) between +200 mV and -200 mV at 100 mV/s, as in [1]. CVs taken at t = 0 (blue) and t = 35 min (red, after being held at +600 mV for 25 minutes) are included at the bottom; moderate binomial smoothing was applied (Igor Pro 6 Wavemetrics) to filter out the current noise and clarify the trend. Initially, the capacitance was 2.5 $\mu$F/cm$^2$ and matched that of [1] for a well-formed monolayer. After application of +600 mV, the capacitance was measured every 5 minutes for 25 minutes, when a maximum capacitance of 3.1 $\mu$F/cm$^2$ was recorded. This indicates that the vast majority of the monolayer was not oxidatively desorbed at these values as the capacitance is significantly lower than that of bare gold [2,3]. Diameter of working electrode was 0.756 cm.
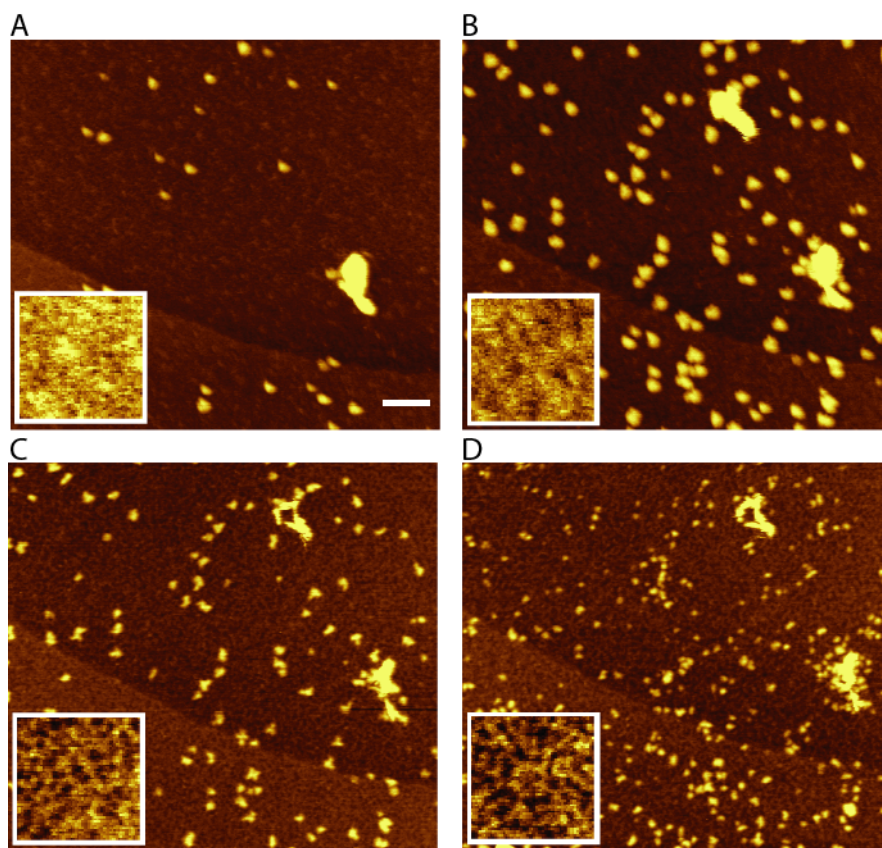
Figure S3: Evolution of switchable monolayer of 503 bp DNA on 6MH subjected to harsh electrode potential cycling from 0 mV to 800 mV and back. Scale bar is 100 nm. Inset: enhanced images of 6MH monolayer from their respective frames. Inset images have the same height contrast, and width of inset images is 100 nm. (A) After briefly applying +600 mV, tethers are still visible across the surface. (B) After repeatedly cycling with harsh potentials, the integrity of the monolayer begins to degrade with a coincident increase in the number of amorphous particles. (C) As the monolayer degrades futher with continued cycling the number of particles remains the same. (D) As defects begin to dominate the surface we see a sharp increase in the number of small particles but only in the area surrounding where amorphous particles had previously been imaged, which suggests that the DNA molecules might be making multiple, yet strong, contacts with the surface through defect sites. Depths of the pits in the monolayer are as large as 0.8 nm, which is significantly larger than the 0.23 nm vacancy islands in the gold substrate and suggests that the MCH molecules are oxidatively desorbed in these regions. Such morphological changes do not appear to be a roughening of the gold because the gold step edge in the frame undergoes no structural transformations. This experiment proves that significant oxidative desorption should be observable by AFM.

# 3 Additional Images and Controls of Switching Behavior of 103 bp DNA Monolayer on MCH
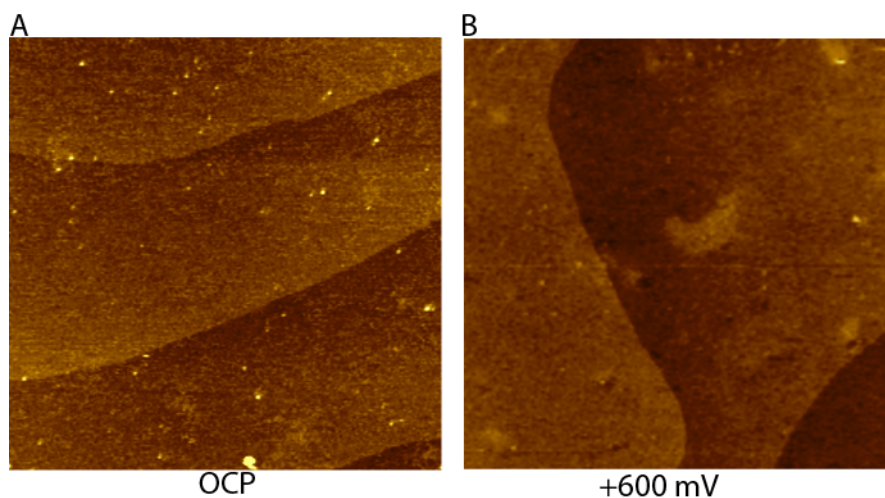


Figure S4: A pre-formed MCH monolayer is exposed to a solution containing unthiolated, 94 bp DNA for 2 hours. The surface was rinsed with copious amounts of TAE solution to remove non-specifically adsorbed DNA, then subjected to +600 mV for several scans. (A) At OCP, the surface appears empty except for a few small protrusions. (B) After three scans while being held at +600 mV, the surface still appears undecorated, with no new protrusions visible, and no noticeable structural changes. Although the sequence is different than the 103 bp DNA, MCH SAM resists non-specific adsorption of unfunctionalized DNAs irrespective of sequences. The lack of adsorption of 94mer is sufficient to confirm that unthiolated dsDNAs do not interact strongly with an OH terminated SAM and are washed away during rinsing.
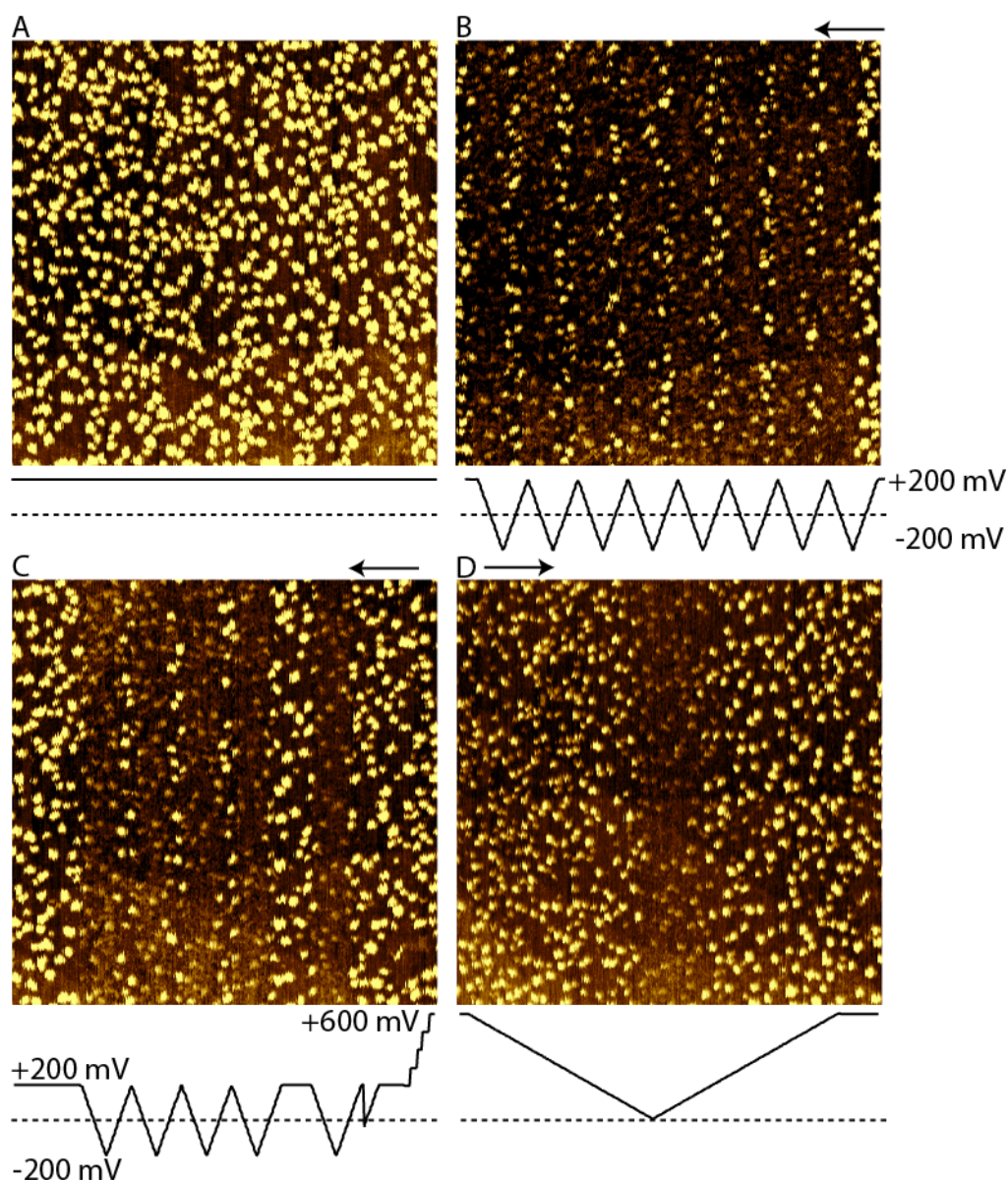
Figure S5: Switchable monolayers of short (105 bp) DNA before and during operation. (A) After holding at +600 mV (see Figure S1), the switchable monolayer is held at +200 mV during the entire scan (uncropped version of Figure 2B). (B) The monolayer is then immediately imaged again while the applied potential is cycled between +200 mV to -200 mV at 25 mV/sec. Time axis increases proceeding left (uncropped version of Figure 2D). Figure S5A and S5B are overlaid in Figure S7 to reveal a molecule-to-molecule correspondence of switching features. (C) Surface is held at +600 mV pprior to scan from right to left, then potential is stepped down to +200 mV. Electrode potential is then scanned once from +200 mV to -200 mV and back at 25 mV/sec, then four more times after a short pause. (D) Switchable monolayer with applied potential cycled between +600 mV to 0 mV and back at 5 mV/sec. Note that lift and re-adsorption do not occur at the same potential, as is the case when cycling at faster rates.
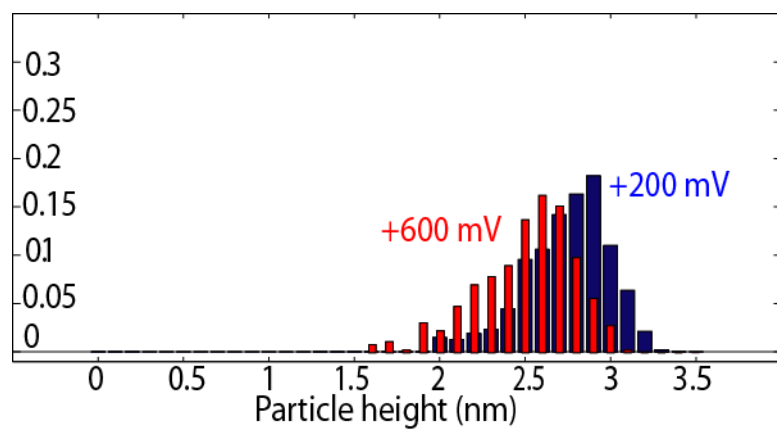
Figure S6: Height histogram of DNA molecules held at +200 mV (from Figure 2B and S5A) and at +600 mV.
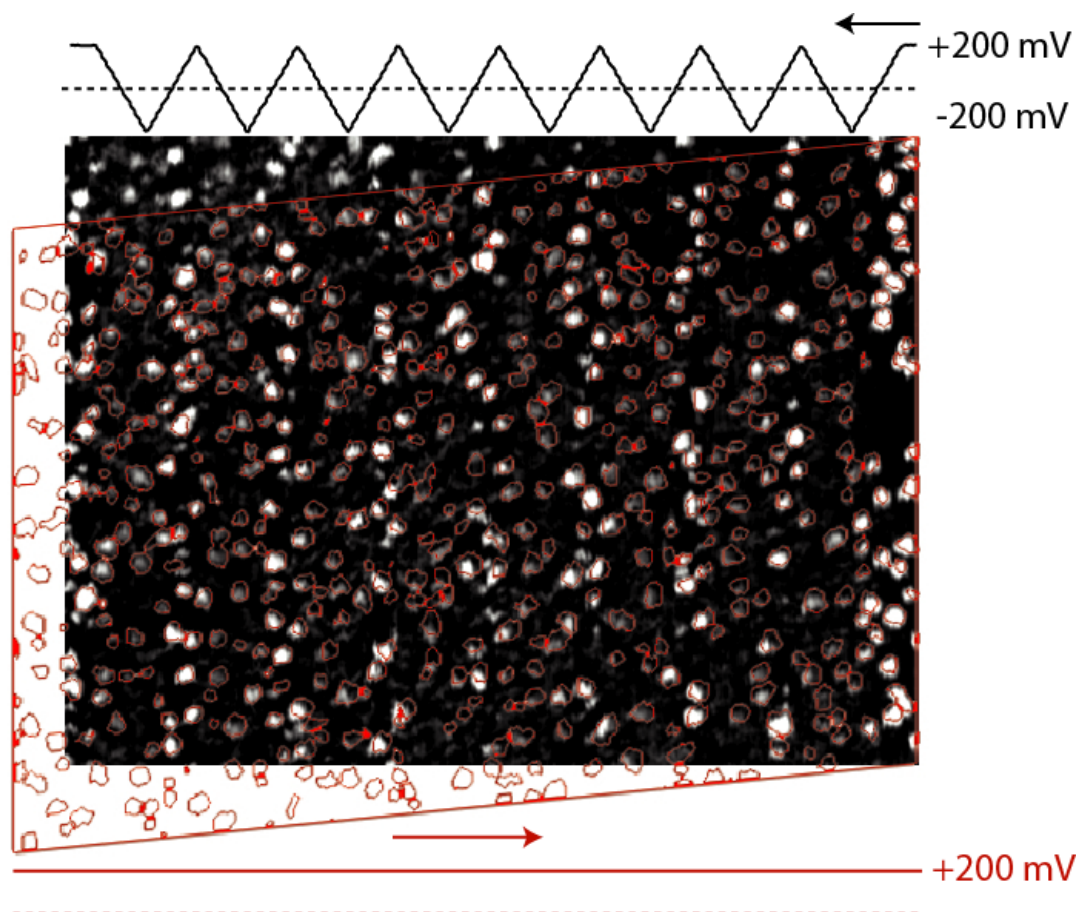
Figure S7: DNA molecules remain at the same location during potential cycling. The surface was first scanned while held at +200 mV (red, from Figure S5A, cropped at the gold step edge along the bottom of the figure), then immediately scanned in the opposite direction while cycling the potential between +200 mV and -200 mV at 25 mV/sec (high contrast grayscale, from Figure S5B). The outline of the strongly adsorbed molecules observed in Figure S5A (red) are then aligned with the desorbing/readsorbing molecules in Figure S5B after compensating for microscope drift. Both the strongly adsorbed (brighter) and lifted (darker, see main text) molecules from S5B appear at the same position where hey were initially imaged in Figure S5A, even after 8 potential cycles (far left). This indicates that even when electrostatically lifted, and only in contact with the surface at their thiol tether, the DNA are not diffusing along the surface. Scan directions (arrows) and concurrently applied potentials indicated for Figure S5A and S5B below and above the figure, respectively.

# 4 Finite Element Analysis of Electric Field Distribution in Switchable DNA Monolayers

A finite element analysis of the electric field distribution was performed using `pdetool` package in MATLAB. The two-dimensional models of a monolayer with a 2.0 nm-wide or 2.5 nm-wide defect was input according to the parameters in Figure S8 through the mid-point of a defect in the monolayer. A modified Poisson-Boltzmann equation [4] which takes into account the size of the counter-ions in confined spaces was used for 0.5xTris acetate, where the size of the counter electrolyte was used to determine the electric field in solution. The electric field in the monolayer was determined by the solution of the Poisson equation equation, assuming relative permittivity of 2.25 and a thickness of 1.02 nm for MCH. [5].
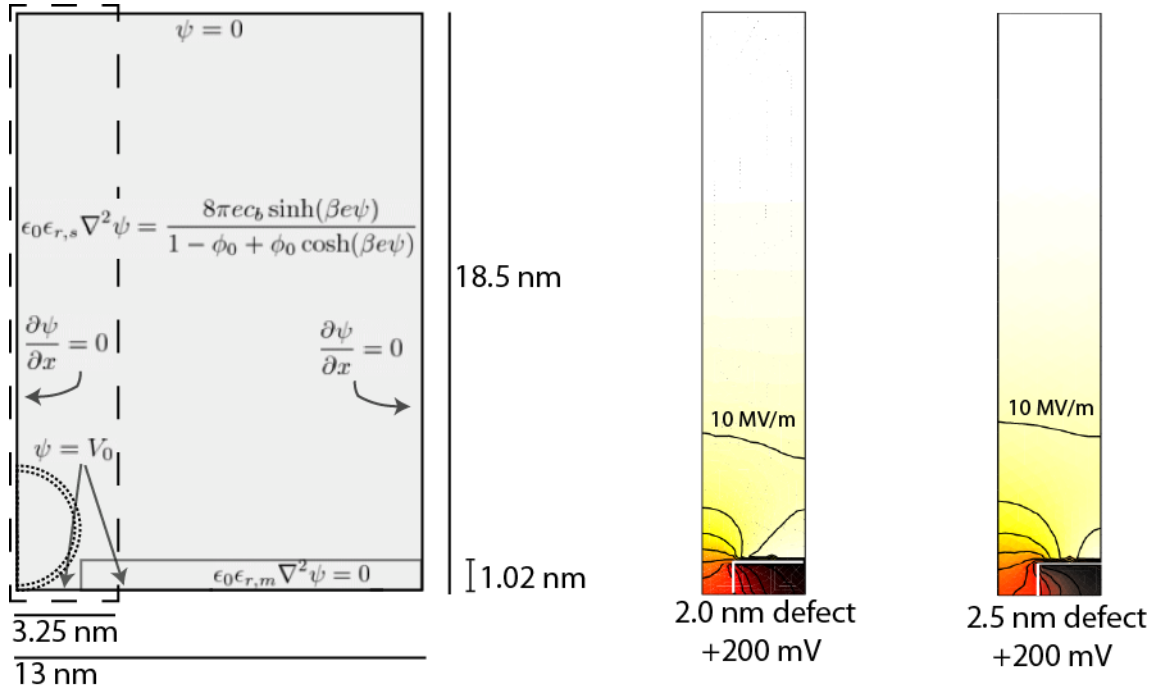


Figure S8: Finite Element Analysis of electric field distribution modeled at a defect site in MCH. See description and specifications in the main text. (left) Schematic of 2-dimensional configuration making use of the bilateral symmetry of the system. Larger area corresponds to area used to model potential distribution used in Figure 5C. Dashed lines correspond to a cropped area for which the electric field distributions are displayed. (middle) Electric field distribution at 2.0 nm-wide defect site in a MCH monolayer at +200 mV (discussed in text for 103 bp DNA). Each line inward from the marked equi-field line represents an increase of 10 MV/m in magnitude. (right) Electric field distribution at 2.5 nm-wide defect site in a MCH monolayer at +200 mV. This is the electric field distribution of the model shown in Figure 5C.

# 5 Estimated Electrostatic Forces

Forces on the DNA were estimated by integrating the electric field in the area of a 0.25 nm ring of inner radius 1.00 nm (Figure S8 left), an approximation for the backbone of a B-DNA double helix, and multiplying by the effective (compensated) charge along the backbone of the DNA at each base-pair from Manning condensation [6] per unit length. This was performed in the case where the DNA is laying flat within an MCH defect 2.5 nm wide, as in Figure S8 at +200 mV, as well as atop a pristine monolayer (no defects) of MCH which is also at +200 mV. We recognize that the presence of the DNA within the defect will dramatically affect the electric fields and distribution of ions in solution, but this exercise is meant as a first approximation to get a rough estimate of the effect of defects on the attractive electrostatic forces applied by the potential; we expect this largely underestimates the electric fields exerted on the DNA in the defect. We find that the forces per unit length felt by the DNA within the defect is 22.8 pN/nm (toward the electrode), while atop a pristine 6MH monolayer the forces fall to 1.8 pN/nm. For the 105 bp DNA, taking the cross-sectional width of DNA as 2.5 nm, we see that at +200 mV the pressure applied by the DNA is $\approx$ 700 kPa, far less than the GPa pressure required to restructure a highly-ordered alkanethiol monolayer by applied mechanical force [7].

# 6  Calculation of Diffuse Layer Potential $\psi_D(V)$ and Surface Charge Density $\sigma_s(V)$ of a Pristine MCH Monolayer, and Estimation of Boltzmann Factor $\hat{g}(V)$ for Fraction of Mobile DNA Close to Surface
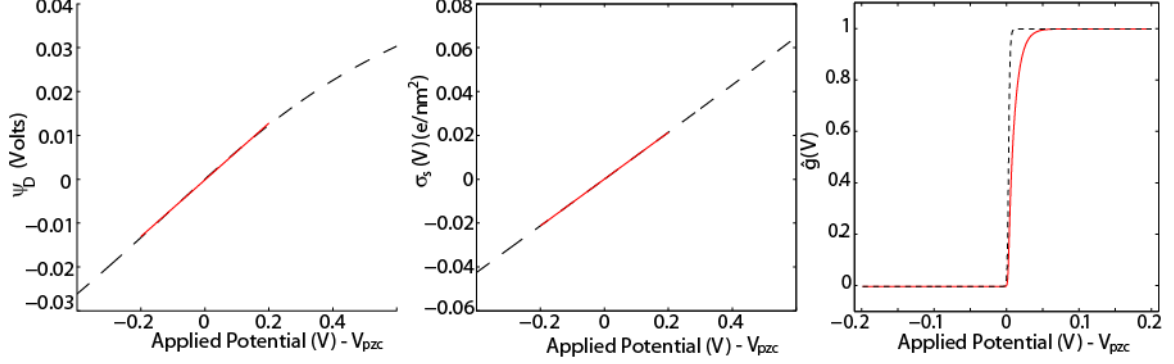


Figure S9: Calculated (left) diffuse layer potential $\psi_D$, (middle) surface charge density $\sigma_s$, and (right) estimated fraction of adsorbed DNA $\hat{g}$ at different applied potentials, above a monolayer of MCH in 0.5x TAE solution. For $\psi_D$ and $\sigma_s$, dotted lines are calculated values and red lines are linear fit between +200 mV and -200 mV. For $\hat{g}(V)$, the dotted black line shows the fraction of DNA molecules whose free end is within one Debye length (2.7 nm) of the surface, while the red shows the fraction of molecules whose free end is within 0.311 nm of the surface.

Solving the Henderson-Hasselbalch equation to determine the concentrations of charged species in 0.5xTAE yields 11.5 mM Tris$^+$, 10 mM Ac$^-$, 0.5 mM EDTA$^{3-}$ at pH 8.13, giving a Debye length [8]:

$$\kappa^{-1} = \sqrt{\frac{\epsilon_0 \epsilon_{r,s} k_B T}{N_A \left(\sum_{i=1}^n c_{\infty i} z_i^2\right)}} = 2.7 \text{ nm} \tag{1}$$

$\epsilon_0, \epsilon_{r,s}, N_A, n, c_{\infty i}$, and $z_i$ are the vacuum permittivity constant, the relative permittivity of the solution (80.1), Avogadro's number, the number of different charged species in solution, the bulk concentration of each of those species, and the charge of each of those species, respectively.

Rant et al. [9] had previously estimated the average orientation of the lifted DNA $\langle \phi \rangle$ in response to applied potential– they could estimate this angle with reasonable accuracy, which was found to be dependent only on solution Debye length $\kappa^{-1}$ and diffuse layer potential $\psi_D(V)$– and following their derivation we assume that the DNA behaves as a charged, rigid rod attached at one end to a surface. More specifically we model the DNA as a series of point charges periodically spaced along a line with distance between base-pairs $b_d$, whose azimuthal angle $\phi$ is dominated by the balance between electrostatic and entropic forces; because the persistence length of double stranded DNA is $\approx 50$ nm and 105 bp DNA is $\approx 33$ nm long a rigid rod should be an appropriate simplification. $\hat{g}(V)$, the fraction of DNA molecules in state W* (at orientation $\phi \to 0$, the original state

W, on MCH) at voltage V, can thus be calculated by the equation:

$$\hat{g}(V) = \frac{\int_0^\epsilon \cos(\phi) \exp\left(\frac{-E(\phi,\psi_d(V))}{k_B T}\right) d\phi}{\int_0^{\pi/2} \cos(\phi) \exp\left(\frac{-E(\phi,\psi_d(V))}{k_B T}\right) d\phi} \tag{2}$$

$$E(\phi, \psi_d(V)) = \sum_{j=0}^{\ell_c/b_d} z_M \psi_D(V) \exp(-\kappa^{-1} j b_d \sin(\phi)) \tag{3}$$

$\ell_c, b_d$, and $z_M$ are the contour length of the DNA, distance between charges along the representation of the molecule (assumed to be distance between base-pairs), and the effective (compensated) charge along the backbone of the DNA at each base-pair from Manning condensation [6], respectively. $\epsilon$ is the (small) maximum angle for which we take the DNA to be close enough to the surface to be able to transition to the strongly adsorbed state; the red line in Figure S9 assumes $\epsilon = 1.09^o$, so that the free end is within 0.311 nm from the surface (assuming the DNA acts as a rigid rod) and within the range of van der Waals forces along its entire length. $\hat{g}(V)$ was estimated numerically by calculating $E(\phi, \psi_d(V))$ for $\phi$ from 0 to $\pi/2$ at every 0.01 degrees, then numerically integrating according to Equation 2 for applied potentials from -0.2 to 0.2 V versus $V_{pzc}$. This estimation of $\hat{g}(V)$ ignores the attractive effects of non-electrostatic terms, but shows that $\hat{g}(V)$ most likely behaves as a step function: for $V > V_{pzc}$, $\hat{g}(V)$ approaches 1 very quickly (all the DNA lie flat on the surface), while for $V < V_{pzc}$, $\hat{g}(V)$ falls to 0 (none of the DNA being in the original W state). To explore the sensitivity to the choice of angle, we calculated the fraction of DNA whose free end remains within 1 Debye length off the surface (the dotted line in Figure S9), and we see that the sensitivity of $\hat{g}(V)$ to changes in $\epsilon$ manifests itself mostly when $V > V_{pzc}$, and any reasonable choice of epsilon would result in a very sharp transition from the lifted state to the mobile state (within 50 mV). This estimation calculates the electric fields atop a pristine MCH monolayer. One complication is that the defects in the SAM may significantly alter the electric field distribution. Nevertheless, the stronger electric fields are expected to result in a sharper transition and hence do not affect our overall conclusion.

# 7 Kinetic Monte Carlo Simulations of Desorption Kinetics During Particle Counting Voltammogram (PCV)

We performed a kinetic Monte Carlo [10] simulation of a PCV experiment during the lifting ('desorption') phase using the following algorithm:

1. Generate the number of DNA that are present on a 'line' (which would be scanned by an AFM) from a random number $N(\mu_0, \sigma_0^2)$, a Gaussian random number with mean $\mu_0$ and standard deviation $\sigma_0$ equal to that of the DNA observed per line when the electrode potential was held at +200 mV during the entire scan (Figure 1D and S5A), rounded to the nearest integer.

2. For each DNA molecule, generate the voltage at which the DNA lifts $V_L$ from a random number generated according to the probability density function (pdf) $f(V)$. $f(V)$ is the pdf of the 'lifting voltage', or the probability that during a PCV experiment where, if the voltage is set to $V_0$ and then is swept at rate $\lambda$ V/s, the DNA lifts between $V$ and $V + dV$. This was accomplished by generating for $V_L$ from a uniformly distributed random number $r$ between 0 and 1 for each molecule (see derivation below):

$$V_L = a - b \ln(-\ln(r)), \tag{4}$$

where parameters $a$ and $b$ are defined below in Equations 16 and 17.

3. The voltages were then sorted and displayed as a PCV, i.e. starting from +200 mV then going to -200 mV at 25 mV/s, displaying the total number of DNA which would be visible on that line at that potential.

The whole process was performed using MATLAB then repeated to simulate multiple 'lines scanned'. This simulation differs slightly from the actual implementation of PCV in that it follows a single line of discrete molecules from the beginning of the experiment until all the molecules have lifted, while in practice we do not observe the same molecule for very long. By aggregating multiple runs of these time courses and 'jumping' from one time course to another one at random every $\approx 10$ mV can be considered approximately what the PCV would look like using a point-like AFM probe.

To generate the probability density function of 'lifting voltages' for individual molecules, we note that rather than using the ensemble kinetics from the previous section, we begin by analyzing the equivalent probability density function of an individual DNA molecule being in state A at time t $P_a(t)$ (during a negative potential sweep starting at positive $V_0$) is (scaling $\delta$ by $k_B T$ to simplify notation):

$$\frac{dP_a(t)}{dt} = -k_d(t)P_a(t) = -\alpha \exp(-\delta(V_0 + \lambda t))P_a(t), \tag{5}$$

We again assume irreversibility of the desorption process from our estimate of $\hat{g}(V)$ and assume a Butler-Volmer-like rate function based on an appeal to the Bell-Evans model (see main text). Both should remain valid in the single-molecule analysis at the voltages

where the DNA lift. Following Laviron's treatment [11] for Butler-Volmer kinetics, the solution to Equation 5 is (noting that $\lambda$ is negative):

$$P_a(t) = C_2 \exp\left(\frac{\alpha}{\lambda\delta}\exp(-\delta(V_0 + \lambda t))\right) \tag{6}$$

where

$$P_a(0) = 1 \tag{7}$$

Rearranging $P_a(t)$ and substituting:

$$a_t = \frac{1}{\lambda\delta}\ln\left(\frac{-\alpha}{\lambda\delta}\right) - \frac{1}{\lambda}V_0 \tag{8}$$

and

$$b_t = \frac{1}{\lambda\delta}, \tag{9}$$

we find:

$$P_a(t) = C_2 \exp\left(-\exp\left(-\frac{t-a}{b}\right)\right) \tag{10}$$

The probability density function of 'lifting times' (time from the start of the experiment to the time the DNA lifts) is $f(t)$; following Kou et al. [12], the probability that the DNA lifts between $t$ and $t + \Delta t$ is $f(t)\Delta t$, which is equivalent to finding the change in probabilities that the DNA is in the 'lifted' states ($P_{w^*}(t) = (1 - P_a(t))$) between $t$ and $t + \Delta t$ ($\Delta P_{w^*}$) over time $\Delta t$:

$$f(t) = \frac{(1 - P_a(t+\Delta t)) - (1 - P_a(t))}{\Delta t} = \frac{P_a(t) - P_a(t+\Delta t)}{\Delta t} \tag{11}$$

Taking the infinitesimal limit (with b < 0):

$$f(t) = \frac{-d(P_a(t))}{dt} \tag{12}$$

$$f(t) = \frac{-1}{b}\exp\left(-\frac{t-a}{b}\right)\exp\left(-\exp\left(-\frac{t-a}{b}\right)\right) \tag{13}$$

Note that $f(t)$ takes the form of a Gumbel distribution [13, 14], often encountered in extreme value theory, and as such the mean time of lifting and variance of the lifting times are:

$$\langle t \rangle = a + \Gamma_0 b \tag{14}$$

$$\langle t^2 \rangle = \frac{\pi^2 b^2}{6} \tag{15}$$

where $\Gamma_0$ is the Euler-Mascheroni constant ($\approx 0.577$). To generate the lifting voltages according to $f(t)$ we change variables to $f(V)$ and integrate to get the continuous density

function, which is then set equal to a uniformly distributed random number $r$ between 0 and 1. Solving for $V_L$ [10] yields Equation 4. Note that after change of variables:

$$a_v = a = \frac{1}{\delta} \ln \left( \frac{-\alpha}{\lambda \delta} \right) \tag{16}$$

and

$$b_v = b = \frac{1}{\delta}, \tag{17}$$

Thus, assuming heterogeneity in $a$ while holding $b$ constant is equivalent to assuming a distribution in the values of $\alpha = \nu \exp(-(\Delta G^{\ddagger} + F_0 \ell_c \Delta x^{\ddagger}))$, and thus a distribution of the non-electrostatic component of adsorption energy. Additionally note that in effect (from Equations 14 and 15), a change in $a$ results in a linear change in the mean lifting voltage for that individual DNA (for large $\delta$, $a \approx \langle V_L \rangle$) as a result of non-electrostatic factors (its local chemical environment), while a change in $b$ $(1/\delta)$ is a change in the standard deviation of the lifting voltages (how sharp the transition between A and W* is). Figures 3B-D each contains 100 runs of the simulation overlaid using different magnitudes and distributions of free energies for each DNA as described in the figure.

# 8 Treatment of Re-adsorption Kinetics during PCV; Justification for Irreversibility Assumption during Lifting Sweep of PCV

In the case of the lifting phase of a PCV, we have argued based on our estimations of $\hat{g}(V)$ that lifting could be treated as irreversible to aid in our analysis. We can no longer argue that the process is irreversible when examining the re-adsorption kinetics during a PCV (we perform a positive potential sweep from a very negative potential at which all DNA begin lifted). As a result, we describe the readsorption kinetics beginning with Equation 7 from the main text, after change of variables:

$$\frac{d\theta_a(V)}{dV} = -\frac{k_d(V)}{\lambda}\theta_a(V) + \frac{k_a(V)}{\lambda}\hat{g}(V)(\theta_T - \theta_a(V)) \tag{18}$$

The $\hat{g}(V)$ term complicates extraction of true rate constants (and perhaps attempts to relate these terms to free energy differences in adsorption) from the PCV data of readsorption. The sharpness of the readsorption transition relative to that of the desorption PCV suggests that the weakly-bound state W may be decoupled from the heterogeneous chemical environment on the surface. This may also be understood in terms of $\hat{g}(V)$: because of the narrowness of the range where we observe the transition to re-adsorption, it may be that the main factor preventing re-adsorption is the low population of DNA near the surface. At potentials where it is more energetically favorable for the DNA to finally approach the surface, the transition rate to strong adsorption at those potentials may already be very large and overwhelm any effects we see from heterogeneity in the surface.

We can still estimate the readsorption rate from the PCV data. We assume that, even while we argue that our interpretations of specific parameters are complicated by heterogeneity of the parameters in the previous section, in the ensemble the first half of the right side of Equation 18 (the desorption rate) is still well-described using the parameters extracted from the fit of the desorptive PCV data. Thus by fitting the $\theta_a$ we observe during the 'readsorption phase' of the PCV with an empirical sigmoidal function $\theta_a(V) = c_0 + c_1/(1 + \exp(V_{1/2} - V)/r))$ (and rate $d\theta_a(V)/dV = c_1/(2r(\cosh((V_{1/2} - V/r) + 1)))$ we can estimate the readsorption rate by rearranging Equation 18:

$$\lambda\frac{d\theta_a(V)}{dV} - \alpha\exp(-\delta V)\theta_a(V) = k_a(V)\hat{g}(V)(\theta_T - \theta_a(V)) \tag{19}$$

We refrain from over-interpreting this fitting of our limited data in this initial study. Nevertheless, we can compare this term with the desorption rate and justify our 'irreversible desorption' assumption in the previous sections. We find that the desorption rate is 10x the readsorption rate at 108 mV, 100x at 38 mV, and over 1000x at -30 mV, and since from the DNA desorption PCV we do not see significant desorption at potentials > 38 mV our simplifying assumption irreversible desorption is justified to a reasonable degree.

# 9 Tracking the Evolution of 503 bp DNA Molecular Structures on MCH Monolayers
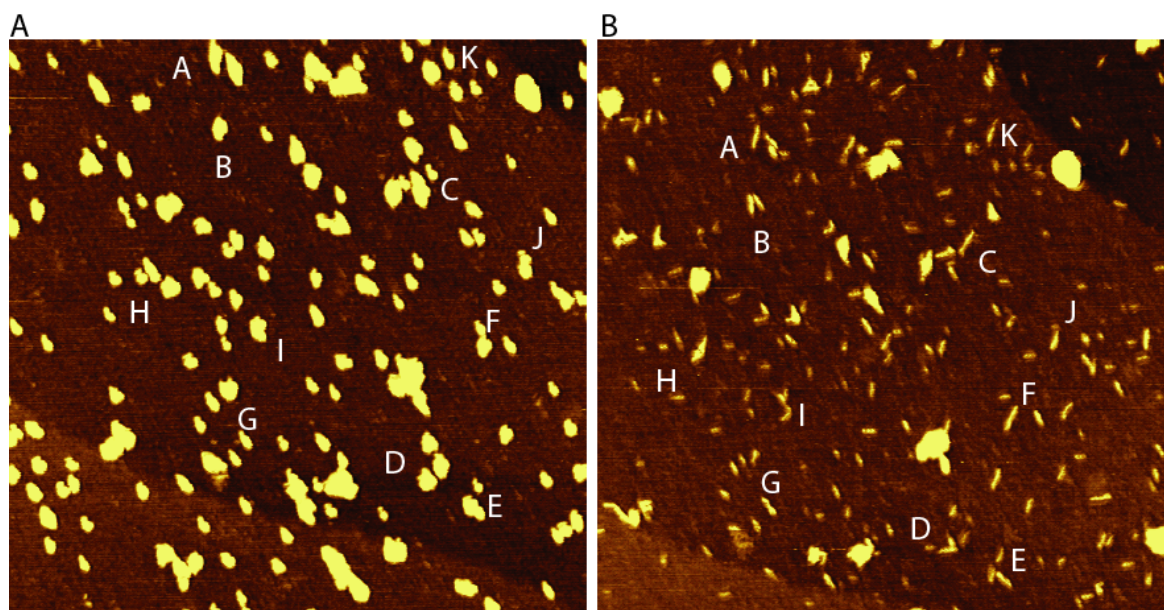


Figure S10: Switchable monolayers of long (503 bp) DNA on MCH before and after potential cycling between +200 mV and -200 mV (uncropped images from Figure 5B and 5D). Letters correspond to tracked features in Figure S11. (A) After initial application of +600 mV, at +200 mV the long DNA initially appear tall and rounded. (B) After cycling the potential several times between +200 mV and -200 mV, long DNA molecules appear on the surface at the heights expected for DNA lying flat atop the gold electrode but embedded within the monolayer. Images are 1 $\mu$m by 1 $\mu$m.

There are 9 frames between Figures S10A and S10B (uncropped versions of Figures 6B and 6D). Additional examples of tall and rounded features being converted into rod-like DNA on the surface (corresponding to the marked letters above) through the course of those frames are shown in Figure S11. These individual protrusions were tracked and aligned from frame to frame using the drift-compensating protocol of Mantooth et al.; see References [15, 16] for details. The sequences of the potentials which were applied between frames was as follows:

**Between top frame (Frame 1) and the one below it (Frame 2):** surface was held at +200 mV.

**Between Frame 2 and Frame 3:** repeatedly cycled between +200 mV and -200 mV.

**Between Frame 3 and Frame 4:** repeatedly cycled between +200 mV and 0 mV.

**Between Frame 4 and Frame 5:** repeatedly cycled between +200 mV and 0 mV.

**Between Frame 5 and Frame 6:** surface was held at +100 mV.

**Between Frame 6 and Frame 7:** repeatedly cycled between +200 mV and -200 mV.

**Between Frame 7 and Frame 8:** repeatedly cycled between +200 mV and -200 mV.

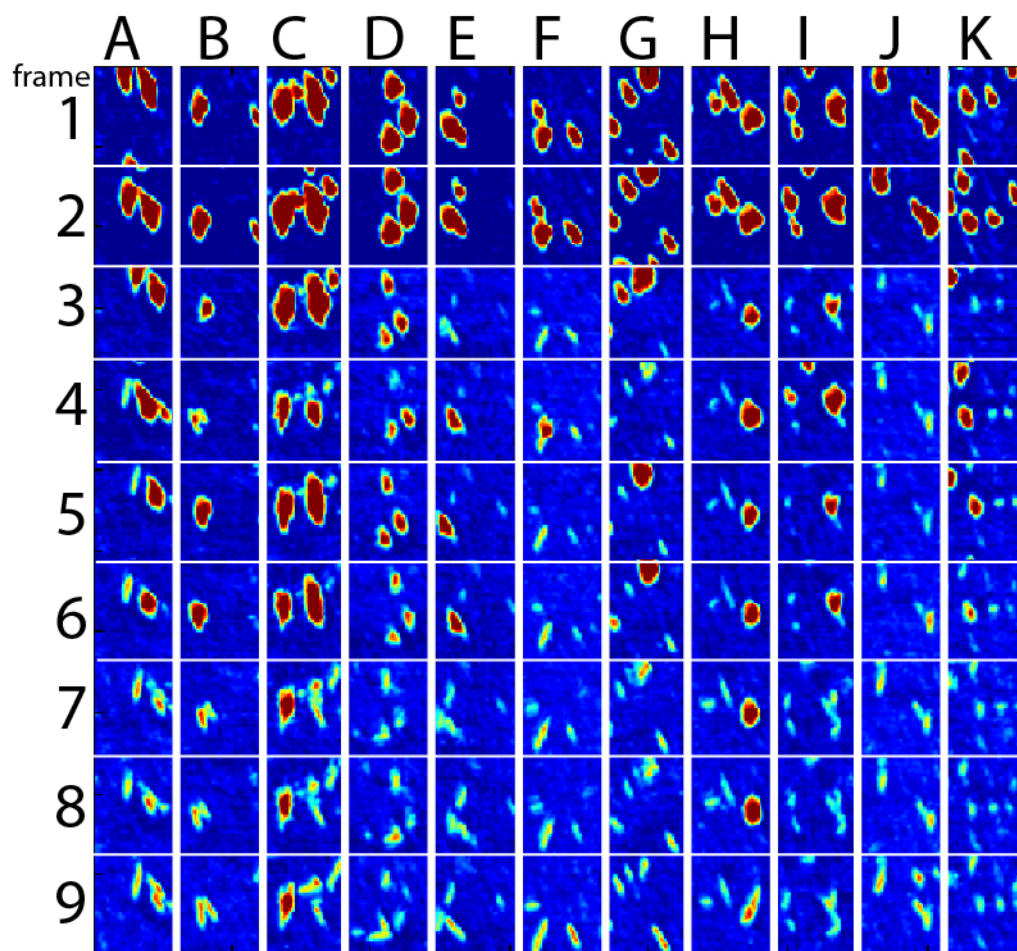**Between Frame 8 and Frame 9:** repeatedly cycled between +200 mV and -200 mV.

Figure S11: DNA molecules tracked and aligned between 9 consecutive AFM scans between which the potential was repeatedly cycled between +200 mV and -200 mV. Nearby letters refer to the DNA molecules in the frames below corresponding to those features in Figure S10. Protocol of potentials applied is described above.
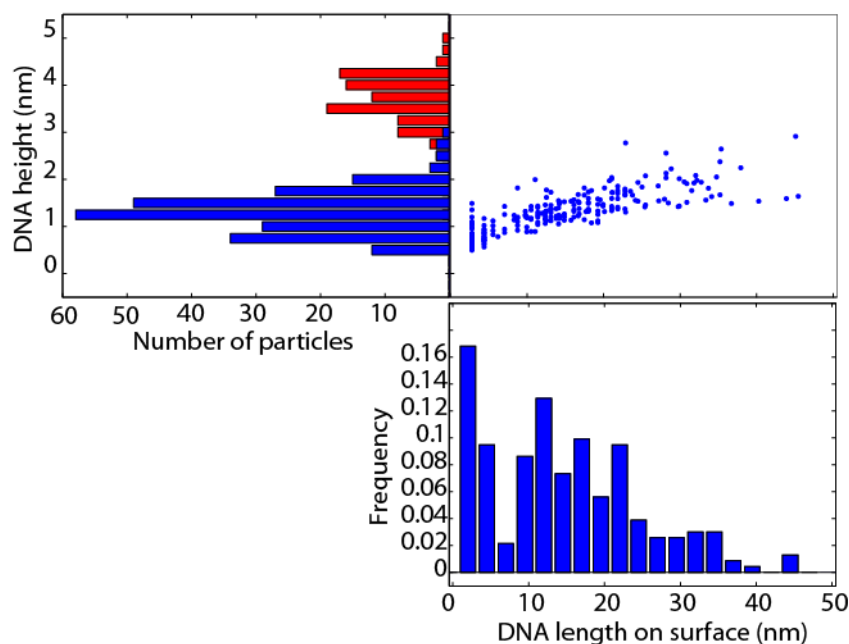
Figure S12: Histograms of the heights (before and after) and lengths (after) of the DNA features before (red) and after (blue) embedding within the monolayer.

# References

[1] C. A. Widrig, C. Chung, and M. D. Porter, "The electrochemical desorption of n-alkanethiol monolayers from polycrystalline au and ag electrodes," *Journal of Electroanalytical Chemistry and Interfacial Electrochemistry*, vol. 310, pp. 335–359, Jul 25 1991.

[2] D. Kolb and J. Schneider, "Surface reconstruction in electrochemistry: Au(100-(5 x 20), au(111)-(1 x 23) and au(110)-(1 x 2)," *Electrochimica Acta*, vol. 31, pp. 929–936, August 1986.

[3] A. Hamelin, "The crystallographic orientation of gold surfaces at the gold-aqueous solution interphases," *Journal of Electroanalytical Chemistry and Interfacial Electrochemistry*, vol. 142, pp. 299–316, Dec 23 1982.

[4] I. Borukhov, D. Andelman, and H. Orland, "Steric effects in electrolytes: A modified poisson-boltzmann equation," *Physical Review Letters*, vol. 79, pp. 435–438, Jul 21 1997.

[5] P. Ramirez, R. Andreu, A. Cuesta, C. J. Calzado, and J. J. Calvente, "Determination of the potential of zero charge of au(111) modified with thiol monolayers," *Analytical Chemistry*, vol. 79, pp. 6473–6479, Sep 1 2007.

[6] G. S. Manning, "The molecular theory of polyelectrolyte solutions with applications to the electrostatic properties of polynucleotides," *Quarterly reviews of biophysics*, vol. 11, pp. 179–246, May 1978.

[7] G. Liu and M. Salmeron, "Reversible displacement of chemisorbed n-alkanethiol molecules on au(111) surface - an atomic-force microscopy study," *Langmuir*, vol. 10, pp. 367–370, FEB 1994.

[8] J. N. Israelachvili, *Intermolecular and surface forces*. London ; San Diego: Academic Press, 2nd ed., 1991.

[9] U. Rant, K. Arinaga, S. Fujita, N. Yokoyama, G. Abstreiter, and M. Tornow, "Electrical manipulation of oligonucleotides grafted to charged surfaces," *Organic & Biomolecular Chemistry*, vol. 4, no. 18, pp. 3448–3455, 2006.

[10] D. T. Gillespie, "General method for numerically simulating stochastic time evolution of coupled chemical-reactions," *Journal of Computational Physics*, vol. 22, no. 4, pp. 403–434, 1976.

[11] E. Laviron, "General expression of the linear potential sweep voltammogram in the case of diffusionless electrochemical systems," *Journal of Electroanalytical Chemistry*, vol. 101, no. 1, pp. 19–28, 1979.

[12] S. C. Kou, B. J. Cherayil, W. Min, B. P. English, and X. S. Xie, "Single-molecule michaelis-menten equations," *Journal of Physical Chemistry B*, vol. 109, pp. 19068–19081, Oct 20 2005.

[13] A. Mossa, S. de Lorenzo, J. M. Huguet, and F. Ritort, "Measurement of work in single-molecule pulling experiments," *Journal of Chemical Physics*, vol. 130, Jun 21 2009.

[14] H. Yang and X. S. Xie, "Probing single-molecule dynamics photon by photon," *Journal of Chemical Physics*, vol. 117, pp. 10965–10979, Dec 22 2002.

[15] B. A. Mantooth, E. C. H. Sykes, P. Han, A. M. Moore, Z. J. Donhauser, V. H. Crespi, and P. S. Weiss, "Analyzing the motion of benzene on au111: Single molecule statistics from scanning probe images," *Journal of Physical Chemistry C*, vol. 111, pp. 6167–6182, May 3 2007.

[16] B. A. Mantooth, Z. J. Donhauser, K. F. Kelly, and P. S. Weiss, "Cross-correlation image tracking for drift correction and adsorbate analysis," *Review of Scientific Instruments*, vol. 73, pp. 313–317, Feb 2002.